Flow Along Porous Media by Partical Image Velocimetry

S. Saleh, J. F. Thovert, and P. M. Adler
Lab. des Phénomènes de Transport dans les Mélanges, CNRS, Avenue du Téléport, 86360 Chasseneuil du Poitou, France

Velocity measurements near porous media are performed by particle image velocimetry. Fully established laminar flows along flat media are studied and compared with the predictions of classical models. Five types of porous media are investigated. Two-dimensional pictures of the flow, average velocities, and local fluctuations are discussed.

Introduction

The determination of relevant conditions at the boundary of porous media immersed in fluids is a long standing problem which has not yet been solved satisfactorily, though it is of a high theoretical and practical interest. The transfer of a passive solute between an external fluid and the porous media is partly controlled by the flow field.

The literature on this topic has been recently reviewed by Vignes-Adler et al. (1987). The free fluid obeys the Stokes equations of motion, and the fluid in the porous medium obeys Darcy's law. Two major descriptions of the boundary region have been proposed in the literature. Beavers and Joseph (1967) introduced a slip velocity proportional to the velocity gradient in the free fluid. Brinkman (1947) postulated that in the porous medium the pressure gradient was due to a Darcy term and a viscosity term; the boundary conditions between the classical Stokes equation and the Brinkman equation are the continuity of the velocity and of the stress tensor.

These equations gave rise to a number of theoretical or numerical works (Prat, 1989; Larson and Higdon, 1986, 1987), but relatively few experiments concerning flows near porous media are reported in the literature. In addition, only global quantities were measured most of the time. Beavers and Joseph (1967) studied a low Reynolds number flow between a solid and a porous boundary; the total flow was compared to the corresponding flow with two impermeable boundaries. Taylor (1971) and Richardson (1971) describe an experiment where a linear Couette flow was imposed above a grooved disk. They measured the torque required to sustain a given velocity of the moving boundary. Matsumoto and Suganuma (1977) and Masliyah and Polikar (1980) measured the settling velocities of porous spheres. Such global data can only be interpreted in the framework of a predefinite model, but they cannot be used for a direct local verification of the models.

To our knowledge, the only attempt to measure local velocity fields above a porous medium is due to Vignes-Adler et al. (1987). The velocity was measured by Laser Doppler Anemometry (LDA) above and inside a medium composed of deep grooves arranged according to a fractal Cantor set. A thorough numerical study of the same type of flow was conducted.

Note that in all these experiments the porous media were either regular synthetic media, or carefully machined random materials. Thus, the areal porosity was always a step function, providing a natural criterion for positioning a limit between the porous medium and the surrounding fluid.

The purpose of the present work is to compensate for the lack of experimental data by measuring local velocity fields close to and possibly beneath the boundary of random porous media. For this purpose, we use the modern Particle Image Velocimetry (PIV) technique, which allows us to record two components of the velocity in a plane sheet on a single picture. One of the advantages of this method is that the geometry of the medium in the plane sheet is simultaneously recorded. Hence, an *a priori* knowledge of the geometry is not required in contrast to a local measurement method like LDA; of course, this feature is very convenient for random media. Note that if the porous medium is transparent, the velocity can be measured inside it as well (Saleh et al., 1992).

Another advantage of local measurements is that they provide easy access to velocity fluctuations. In the theoretical models, the streamlines are supposed to be rectilinear. In other words, the velocities are averaged at a scale much larger than the typical grain size. For example, the Darcy's seepage velocity filters out the velocity fluctuations within the pore space. These equations might be sufficient to describe the transfer of momentum between the free flow and the porous layer. However, they are certainly unable to describe the transfer of other quantities like heat or solute. Consider, for example, a flow over the infinite plane surface of a porous medium. On the average,

the flow is one-dimensional and the streamlines are parallel to the boundary. In this description, the exchanges of solute or heat between the porous layer and the free flow are controlled by diffusion. However, at a microscopic scale, the velocity close to the boundary has a rapidly varying vertical component, due to the irregular surface of the medium. Hence, a convective transport occurs across the boundary, which is likely to enhance greatly the exchange rate.

This article is organized as follows. The second section briefly recalls the theoretical aspect of the boundary conditions between a free fluid and a porous medium. The models of Beavers and Joseph (1967) and Brinkman (1947) are recalled.

The third section describes the experimental setup and the measurements. A Poiseuille-like flow was generated above a porous medium in a parallelepiped cavity. Care was taken to ensure a fully-established flow in the measurement region. The flow was generated by pressure difference between two constant level tanks. The fluids, either silicone oil or white medicinal oils, were seeded with microscopic particles. The fluid was illuminated by sweeping a laser beam in a vertical plane parallel to the main flow direction. A great improvement was achieved with the use of a moving camera; the ratio between the largest and the smallest measurable velocity was considerably increased and a single picture was sufficient to explore the whole velocity field. Five kinds of porous media were investigated: a synthetic plastic foam, two beds of glass spheres and two beds of random glass grains.

Measurements are gathered and discussed in the fourth section. The profiles obtained with the foam are described first. Because of the machined surface of the porous medium, the departure from the parabolic Poiseuille profile is very small. A comparison is started with the predictions of Beavers and Joseph (1967); however, it cannot be quantified because of the uncertainty in the position of the boundary.

The profiles above the porous medium made of glass spheres were found to be very close to parabolas, when they were spatially averaged in order to take into account the local fluctuations due to the distribution of spheres. It should be noted that the larger beads were almost packed regularly while the smaller ones were randomly packed; no significant differences were seen in the results. It is remarkable to see that the average velocity profiles differ from parabolas only very close to the boundary of the porous medium. More interesting are the profiles of the velocity fluctuations which are found to be maximum at the top of the highest spheres; they decrease on both sides of this level. In the bulk, they are found to be negligible at about one sphere diameter above the maximum.

Finally, measurements were performed over the two beds of random glass grains; the first one is obtained by breaking glass rods and the second one glass plates. Again, a parabolic profile could be fit on most of the profile far from the porous medium. The data were then interpreted in terms of the Brinkman equation with a varying permeability. Because of the relative size of the grains with respect to the width of the channel, the velocity fluctuations were found to be very large, and no plateau was reached far from the porous medium.

General Problem of Boundary Conditions

Consider a Newtonian fluid of viscosity μ which flows in and along a porous medium, as shown in Figure 1a. The perme-

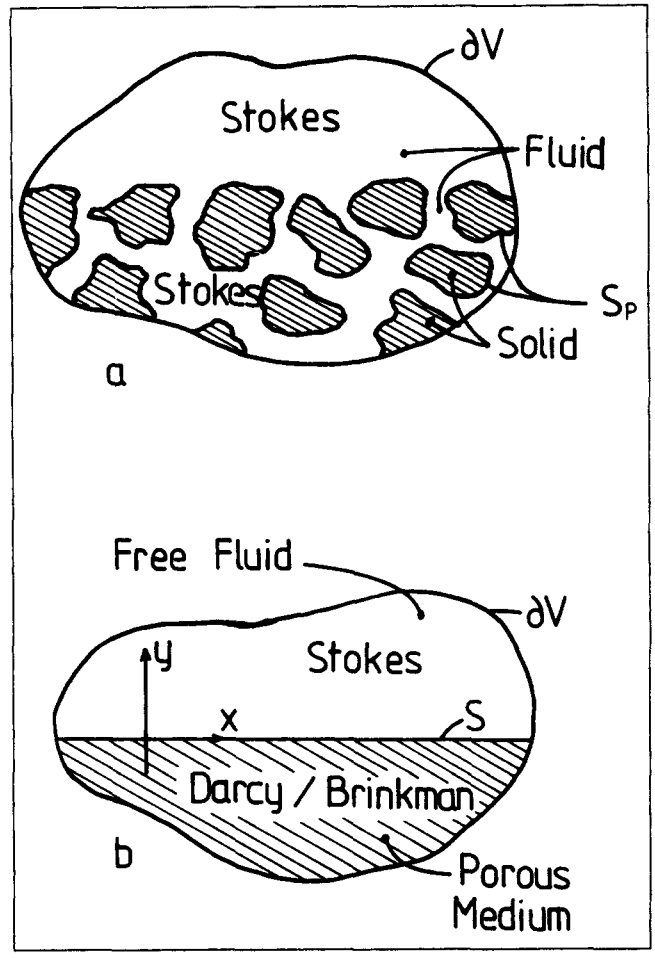

Figure 1. General problem of the boundary conditions at the surface of a porous medium.

In a, the Stokes equation is solved everywhere. In b, the domain is split into two parts which have to be related by adequate boundary conditions.

ability of the porous medium is denoted by K; at the scale 1 of the obstacles or capillaries present in the porous medium, the motion of the fluid obeys the Stokes equations of motion when inertia is neglected:

$$\nabla p = \mu \nabla^2 v \qquad \nabla \cdot v = 0$$
$$v = 0 \quad \text{on } S_p \tag{1}$$

where v, p and S_p denote the velocity, the pressure and the surface of the solid. Adequate external boundary conditions must be added to this set of equations. For instance, pressures and velocities are imposed on some parts ∂V_1 and ∂V_2 of the external boundaries:

$$p = p(x) \qquad \text{on } \partial V_1$$
$$v = v(x) \qquad \text{on } \partial V_2 \tag{2}$$

The system of Eqs. 1 and 2 can be solved in principle, but it represents a formidable problem which can only be successfully addressed in particularly simple cases, such as the ones considered by Richardson (1971), Vignes-Adler et al. (1987), Larson and Higdon (1986, 1987) and Adler (1987).

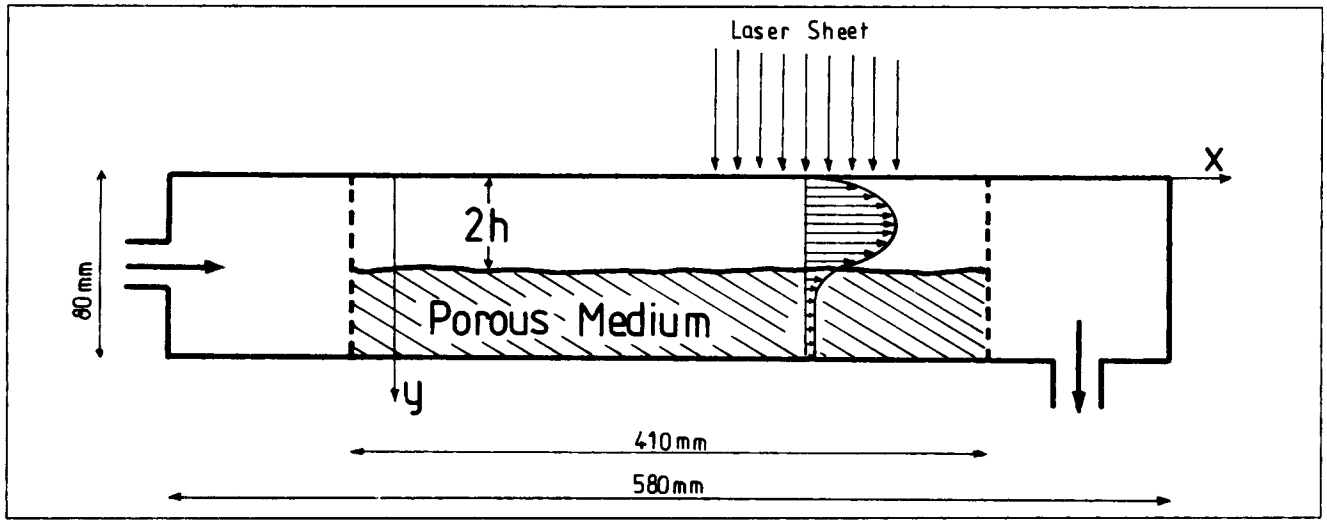

Figure 2. Longitudinal cross section of the experimental cell.

Standard usages are followed in the notations. The velocity averaged in some sense is denoted by an overbar and the corresponding fluctuation by a prime. For instance, we have $v=\bar{v}+v'$. Unless otherwise stated, averages are taken over sets of points at the same elevation y. The x and y components of v are denoted u and v, respectively. Standard deviations are denoted by a double bar, for example, $\overline{\overline{v'}}=\sqrt{\overline{v'^2}}$.

Instead, the situation displayed in Figure 1a can be simplified as follows. Out of the porous medium, the Stokes Eq. 1 is still valid. Inside the porous medium, the average interaction between the fluid and the solid is usually described by Darcy's law:

$$\overline{V_D}=-\frac{K}{\mu}\nabla p \tag{3}$$

where the seepage velocity $\overline{v_D}$ is the volume average of the local velocity v.

The major drawback of this simplification is that boundary conditions at the interface S between the free fluid and the porous medium are now needed, as shown in Figure 1b.

Beavers and Joseph (1967) introduced a slip velocity, which is proportional to the velocity gradient in the free fluid:

$$\left.\frac{d\bar{u}}{dy}\right|_{0^+}=\frac{\alpha}{\sqrt{K}}\left(\bar{u}|_0-\overline{u_D}|_0\right) \tag{4}$$

Where $\bar{u}|_0$ and $\overline{u_D}|_0$ are the x-components of the average velocity in the free flow and of the seepage velocity in the porous medium close to the interface. The origin of the y-coordinate is taken at the boundary of the porous medium. The dimensionless empirical parameter α depends only upon the medium under consideration. The additional boundary conditions are continuity of normal velocity and normal stress.

It is important to observe that Eq. 4 supposes that the position of the boundary ($y=0$) is defined unambiguously. This might be achieved with synthetic or machined media. However, for most natural media, there is no well-defined interface between the porous medium and the free fluid. Various contributions have shown that the parameter α is not intrinsic, but depends on the arbitrary location where Eq. 4 is written. Larson and Higdon (1986) stated, "All reasonable choices for α are equivalent, subject to microscopic changes in the definition of the interface."

For future reference, it is interesting to recall the simple solution of a fully established flow in a channel of height $2h$ above an infinite porous medium. This is illustrated in Figure 2, and it was the situation investigated by Beavers and Joseph (1967). The solution to the Stokes equation in the free fluid with the boundary condition Eq. 4 can be expressed as:

$$u(y)=\frac{1}{2\mu}\frac{dp}{dx}\left[y-2h\left(1+\xi\frac{1+\alpha\xi}{2\alpha+\xi}\right)\right]y \tag{5a}$$

where the origin is taken at the upper wall and ξ is given by:

$$\xi=\frac{\sqrt{K}}{h} \tag{5b}$$

A second classical approach is based on the semi-empirical Brinkman equation (Brinkman, 1947):

$$\nabla p=\tilde{\mu}\nabla^2 v-\frac{\mu}{K}\overline{v_D} \tag{6}$$

which is a superposition of Darcy's law and Stokes equation.

The meaning of Eq. 6 is physically clear. Inside the porous medium, diffusion of momentum, via the effective viscosity $\tilde{\mu}$, is added to the predominant Darcy term. Outside of the porous medium, $\tilde{\mu}=\mu$ and the Darcy term vanishes, yielding the usual Stokes equation. It is not clear which value of the effective viscosity $\tilde{\mu}$ has to be used in Eq. 6. Brinkman took $\tilde{\mu}=\mu$, but other values were proposed in subsequent works; either $\tilde{\mu}=\mu/\epsilon$, where ϵ is the porosity, or equivalently $\tilde{\mu}=\mu$ with v being interpreted in the porous medium as the mean interstitial velocity $\bar{v}^*=\overline{v_D}/\epsilon$. Lundgren (1972) proposed a viscosity which accounts for the solid concentration, similar to

the Einstein's correction for the viscosity of dilute suspensions. Hence, the Brinkman equation is basically an effective medium approximation, and as such its validity is restricted to highly porous media. In this situation, the difference between $\tilde{\mu}$ and μ is at most of order $(1-\epsilon)$.

The Brinkman Eq. 6 can be itself easily solved when coupled to a Stokes equation for a fully-established flow over a flat porous medium of infinite thickness. The flow field can be expressed as:

$$u=\frac{1}{2\mu}\frac{dp}{dx}\left[y-2h\left(1+\xi\,\frac{1+\frac{\tilde{\mu}}{\mu}\,\xi}{2\,\frac{\tilde{\mu}}{\mu}+\xi}\right)\right]y \quad 0\le y\le 2h \qquad (7a)$$

$$u=-\frac{K}{\mu}\frac{dp}{dx}\left[1+\frac{\tilde{\mu}}{\mu}\,\frac{2-\xi^2}{\left(2+\frac{\tilde{\mu}}{\mu}\,\xi\right)\xi}\,e^{(2y-h)/\sqrt{K}}\right]y \quad 2h\le y \qquad (7b)$$

Note that Eq. 7a is equivalent to Eq. 5a with $\alpha=\tilde{\mu}/\mu$.

Another feature has to be considered when one deals with the boundary of a porous medium (near a solid wall or a free fluid). Generally, the porosity is not a step function. The presence of a solid wall modifies the packing density of the solid particles and induces a decrease of the solid concentration, which is turn may create preferential paths for the percolating fluid. Similarly, near the boundary S with the free fluid, except when the surface of the medium has been machined, the porosity increases continuously toward 1; this yields a corresponding permeability increase. These porosity variations are usually confined in thin layers whose thicknesses are of the order of a typical grain size, but these are precisely the regions where the Brinkman correction to Darcy's law is expected to have a sensible influence.

Experimental Setup

Apparatus

The basic principles of the measurement method, as well as a general description of the apparatus involved in the various steps of the procedure were given by Saleh et al. (1992) and Saleh (1993). Therefore, only the specific features of the present application are detailed here. The measurement cell, the hydrodynamic environment and the parameters for the acquisition of the photographic records are discussed, but no detail about the subsequent optical and numerical treatments is given.

The parallelepiped measurement cavity ($560\times206\times80$ mm^3; see Figure 2) is made of polycarbonate plates (Luxan). This material was chosen because it has better optical properties than polymethacrylate (Perspex), especially with respect to aging. In addition, its surface can be treated to enhance its resistance to abrasion. Two vertical grids are set 410 mm apart within the cell. The central part of the cavity, between the grids, can be totally or partially filled with any type of porous material. There are two tranquilization chambers, outside of the grids, at both ends of the cell.

A pressure driven flow is created through the cavity by connecting the inlet and outlet to two constant level reservoirs. The flow rate is measured by a volumetric counter. The Reynolds number of the flow, based on the height of the free channel above the porous medium, is smaller than 1 and typically about 0.5. The fluid is either a Silicon oil (Dow Corning DC 200, $\rho=970$ kg·m^{-3}, $\nu\sim200$ cSt) or a mixture of white medicinal oils (1/3 Esso Marcol 82 + 2/3 Esso Primol 352, $\rho=860$ kg·m^{-3}, $\upsilon\sim100$ cSt). We always operate at room temperature, between 20 and 23°C. The fluid is seeded with small tracers, either aluminum coated spheres (4 μm in diameter, $\rho=2{,}600$ kg·m^{-3}), or silicon carbide particles (typical size 1.5 μm, $\rho=2{,}600$ kg·m^{-3}). The volumic tracer concentration is $9.7\ 10^{-7}$ (that is, 29 particles per mm^3) or $3.1\ 10^{-7}$ (that is, 175 particles per mm^3).

The flow is illuminated by sweeping a laser beam in a vertical plane parallel to the longitudinal axis of the cell. The beam is collimated in order to reduce its diameter to 400 μm in the measurement zones. Two types of light sources have been used. Early measurements were performed with a 25 mW He-Ne laser. Because of this low power, a rapid photographic film was needed. A Kodak TMax-400 ASA 35 mm film was used and processed in the Kodak TMax developer. The larger tracers (4 μm) were used with this source for the same reason. Subsequent measurements were performed with a 3 W Argon laser. This substantial increment of the source intensity allowed the use of the smaller tracers (1.5 μm) and of a slower photographic film. Smaller particles are desirable, because they have a lower settling velocity. Note that the settling of the 4 μm particles is always smaller than 1 μm/s and does not bias the velocity measurements. However, the deposition of the tracers on the solid surfaces over long periods of time has several drawbacks, since it may induce a higher noise level in some regions of the domain. On the other hand, slower films generally present a finer resolution. The ultrafine grain Kodak film Technical-Pan 2415 was used and processed in the Kodak HC 110 developer (1 + 11.5 dilution, 8 mn at 20°C). This process yields a 125 ASA speed and a very high contrast index ($\gamma=1.80$).

The precision of the focusing of the photo camera on the plane of illumination is a crucial point for obtaining a suitable record. With the 55 mm Nikkor lens, the $f^{\#}=8$ stop number, and the range of magnification M used for all the measurements, the depth of field is smaller than 1 mm. The automatic focusing of the Nikon F4 camera was always found to be far more accurate than a manual one. Images of the tracers on the film were about 30 μm, which is close to the diffraction limit $2.44\ (1+M)\ f^{\#}\ \lambda\approx15$ μm, whereas a careful manual focusing on a ruler inserted in the light sheet, with the help of a $\times6$ magnifying viewfinder resulted in a typical size of 100 μm.

Two different methods have been applied to cope with the wide range of velocities in the measurement zone. Recall that the time interval between two successive exposures has to be adjusted (via the frequency of the beam sweep) to the velocity range in order to keep the spacing of the tracer images in a suitable span. A practical range is $30\sim300$ μm, which corresponds to a maximum ratio of 10 between the largest and the lowest velocities measurable on a same record. In the present type of flow, where the center of the channel, the vicinity and even the interior of the porous medium are interesting, this limitation is severe. This problem was solved in the first series of measurement by making two separate records of the same flow with different frequencies. Each record provides infor-

mation on the velocity in different and overlapping regions. This technique has several drawbacks. First, it increases the number of manual operations in the subsequent treatment of the records. It also requires an accurate measurement of the positions. Finally, although this has no incidence in the present stationary case, it cannot be applied to unsteady flows.

In the second series of measurements, a more convenient method was used. In Laser Doppler Velocimetry, the velocity field can be artificially shifted by a Bragg cell. Here, the shift is obtained by translating the camera during the photography, at a steady speed v_s in the direction opposite to the flow. By an adequate velocity shift, the dynamic of the apparent velocity field can easily be decreased below 10; thus, it becomes possible to measure the whole velocity field on a single record. It is of course an easy matter to substract v_s in the subsequent treatment and to recover the actual velocities. This method has an additional advantage, which is of little use here; when inversions of flow occur, it can resolve the ambiguity on the sign of the velocity.

Moving the camera is the crudest way to make a velocity shift, and various other methods have been proposed. However, because of the size of the experimental cell and of the range of magnification in this application, the lens of the camera is put very close to the wall of the cell, and this prohibits the use of a rotating mirror. Since the intermittent planar illumination is obtained by sweeping an unmodified beam, instead of chopping a beam expanded in one direction by a cylindrical lens as is commonly done, the electrooptical method of Landreth and Adrian (1988) cannot be applied.

Note finally that for practical convenience, the investigated volume is often out of the central part of the channel. This is not expected to induce any significant side wall effects, since the exact solution (Berker, 1963) of the Stokes equation in a rectangular pipe 206 mm wide and 40 mm high (which is the typical height of the free channel) shows that the velocities in a vertical plane at one-fourth (respectively one-third) of the channel width never differ from those in the central section by more than 1.8% (respectively 0.5%). In the x direction, the measurement window is centered at about 300 mm (that is, about 7.5 channel heights) from the upstream grid; hence, the influence of the entrance conditions (initial step, grid) is damped out and the flow pattern is fully established.

Porous media

Five kinds of porous media were investigated, namely a synthetic plastic foam, two beds of glass spheres, and two beds of irregularly shaped glass grains.

The synthetic medium is a polyurethane foam (Bulpren S10, manufactured by Sofiltra-Poelman, France). This material was designed for air-filtration purposes. It is a reticulated foam, that is, only the edges of the cells remain in the final product (Figure 3). Its porosity and permeability are very high: $\epsilon \sim 0.97$, $K \sim 10^{-8}$ m^2. The typical size of a cell ranges from 2 to 5 mm. The foam swells slightly when it stays in Silicon oil for a long time. A $208 \times 40 \times 410$ mm^3 parallelepiped was cut out of a larger sample.

The earlier measurements (with the low power light source and without any velocity shift) were performed with this foam and silicon oil. All the following media were studied with the mixture of white medicinal oils, the 3 W laser and the velocity shift.

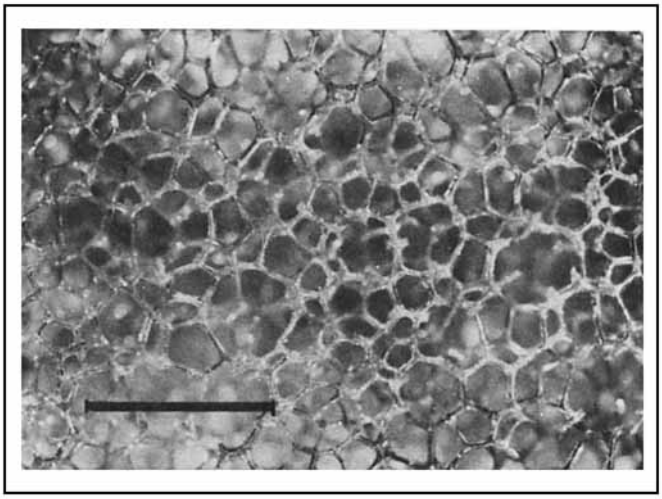

Figure 3. Sample of synthetic foam Bulpren.
The length is 1 cm.

Two beds of glass beads were used. The bead diameters are 6 mm and 10 mm. The larger ones were packed tentatively in a regular hexagonal pattern. Five layers were arranged manually. However, because of the poor sphericity of the beads, the order in the upper layers is only approximate. The particles in the superficial layer are still approximately distributed according to an hexagonal lattice, but they are not all at the same elevation (Figure 6). The smaller beads were packed randomly. The porosity of both packings was measured by saturating a known volume with oil. The ordered packing has a porosity $\epsilon \cong 0.34$ and the random one $\epsilon \cong 0.40$. Their permeability was not measured directly but estimated by the empirical relation of Rumpf and Gupte (1971) which results from the compilation of experimental data for random packings of spheres:

$$K \approx \frac{D^2}{5.6}\,\epsilon^{5.5} \tag{8}$$

where D is the average sphere diameter. This yields $K \cong 5.10^{-8}$ m^2 for the larger beads and $K \cong 3.10^{-8}$ m^2 for the smaller ones.

It was not possible to adjust the refractive indices of the solid grains and of the fluid. There are two reasons for that. First, the optical index of ordinary glass is relatively high ($n \cong 1.51$). Second the index of the glass varies inside the beads, because of their fabrication (cast). Thus, it was not always possible to measure the velocity down to the surface of the solid grains in the measurement plane, because it was hidden by beads located above the average interface.

Finally, two beds of irregularly shaped glass grains were studied (Figures 9 and 10). There grains were obtained by randomly breaking either rods (10 mm in diameter) or plates (10 mm thick) of borosilicate glass (Pyrex). The porosities of these beds are $\epsilon = 0.38$ (rods) and $\epsilon = 0.425$ (plates). Their permeabilities were measured, and found to be almost identical, $K \sim 10^{-7}$ m^2. The low refractive index of this glass ($n \cong 1.473$) could be easily matched with the index of the fluid. Thus, the velocity could be measured between the solid grains as well.

Note that the five media have comparable permeabilities. The overall range for K is $10^{-7} \sim 10^{-8}$ m^2. Consequently, the

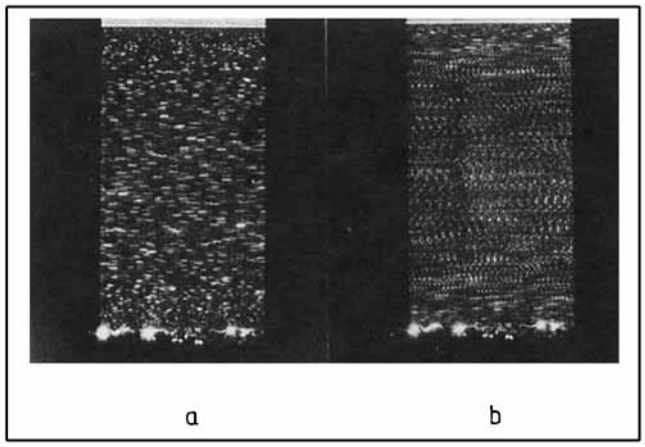

Figure 4. Multiexposure photographs of a flow between a solid wall and a synthetic foam.

The beam-sweep frequency is 5 Hz (a) or 1 Hz (b).

ratio of the seepage velocity in the porous layer to the average velocity in the free channel is always very small (10^{-3} to 10^{-4}).

Results

Plastic foam

In contrast with the four other media, this synthetic material has a fairly regular surface. For this reason, the velocity field above the porous layer was recorded in a single planar window, 20 mm wide, and parallel to the longitudinal axis of the measurement cavity. Since the velocity close to the upper wall or to the porous medium and in the center of the channel could not be measured on a same record, two separate photographs were taken with two beam sweep frequencies of 1 Hz and 5 Hz (Figure 4). The local velocity was measured at 50 successive points separated by 0.8 mm along 30 vertical profiles. The 5 Hz frequency record was used through most of the channel cross-section. Only the two lowest velocities on both sides of the profiles were measured on the 1 Hz record.

The longitudinal component of the velocity, averaged over the 30 profiles is displayed in Figure 5a. Since the flow in the channel is governed by the Stokes equation, a parabolic profile is expected, at least out of the thin layer close to the foam. A parabolic profile was fitted on our data out of this zone close to the porous medium. This was done by a least-square method, in the 35 mm upper part of the channel. The result is displayed in dash line in the figure. The data are indeed very close to the fitted profile:

$$u = u_M \frac{2y}{h'}\left(1 - \frac{y}{2h'}\right) \tag{9a}$$

with

$$u_M = 1.132 \text{ mm}\cdot\text{s}^{-1} \quad 2h' = 39.80 \text{ mm} \tag{9b}$$

In the present situation, the position of an interface between the free flow and the porous medium is in principle defined unambiguously by the cutting plane. Thus, it is *a priori* well suited to a description by the Beavers and Joseph model. According to Eq. 5, one expects a slip velocity u_{sl}:

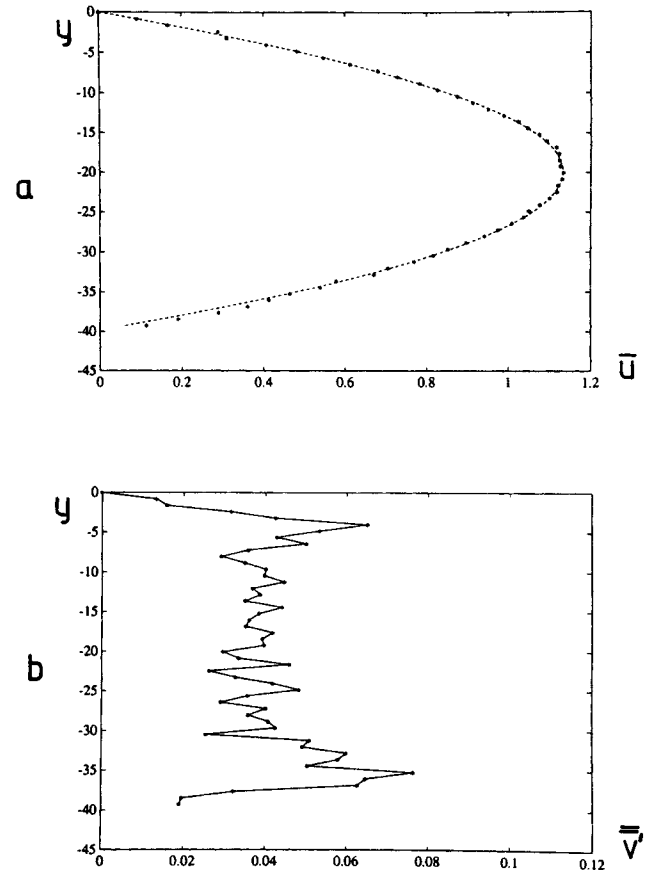

Figure 5. Flow between a solid wall and a synthetic foam.

Distances are in mm and velocities in mm/s. (a) Average longitudinal velocity $\bar{u}$. The dash line is a parabolic profile fitted on the data; (b) Standard deviation of the vertical velocity $\bar{v}'$.

$$u_{sl}/u_M \approx \frac{2}{\alpha}\frac{\sqrt{K}}{h} \tag{10a}$$

where u_M is the maximum velocity, $2h$ is the channel height and α is of the order of unity. With the current values of K and h, this yields:

$$u_{sl} \approx \frac{1}{\alpha}\frac{u_M}{100} \tag{10b}$$

However, even this apparently gentle case was not simple. The channel height was measured by materializing the foam surface by a 26×70 mm^2 microscope object slide; $2h$ was equal to 38.8 mm. The fitted parabolic profile gives, at this distance from the upper wall, $u_{sl}/u_M = 0.098$, that is, $\alpha \approx 0.10$. But as a matter of fact, the slide did not lie on a hypothetical average interface, but rather on top of a few protruding spikes, which were not cut neatly during the preparation of the sample; they have little hydrodynamical influence. Moreover, the swelling of the foam made its surface warp slightly. Hence, this value of h is certainly underestimated. In particular, the lowest points where the velocity was measured, 39.2 mm away from the upper solid wall, are still in the channel.

The distance between the foam and the solid wall was then measured directly on the photographic record (Figure 4), that is, in the region where the velocity measurements were performed. It was found that the fabric of the foam was cut at $2h = 40.1 \pm 0.1$ mm from the upper wall. Note that this small error bar is still of the order of the relevant length scale $\sqrt{K} \approx 100$ μm. The fitted profile (Eq. 9) gives a negative value of the velocity at this value of y, resulting, via Eq. 10, in $\alpha < 0$.

This illustrates the underlying problems when the Beavers and Joseph model is used. At least two conditions have to be met for the parameter α to be defined intrinsically. The porous medium has to be homogeneous, and the location where Eq. 4 is written has to be defined unambiguously at a scale much larger than the typical grain size (or cell size, presently), with an uncertainty lower than $\sqrt{K}$. These two conditions are not fulfilled in the present case; even though the foam was machined, the position of an hypothetical interface is still scale-dependent; moreover, the porous medium is heterogeneous, as made obvious by the net outgoing flux visible in Figure 4b.

The solution (Eq. 7a) of the Brinkman equation can be evaluated with $\tilde{\mu} = \mu$ and the measured values of the channel height $2h = 38.8$ mm and 40.1 mm. It is obtained:

$$u = u_M \frac{2y}{h''}\left(1 - \frac{y}{2h''}\right) \tag{11}$$

where $2h = 38.9$ and 40.2 mm, respectively. The fitted profile (Eq. 9) lies in between these two profiles (Eq. 11). Reversely, the profile (Eq. 9) corresponds to $2h = 39.7$ mm.

The standard deviation $\overline{v'} = \sqrt{\overline{v'^2}}$ of the fluctuation v' of the vertical velocity is displayed in Figure 5b. It is fairly constant through most of the channel. This plateau corresponds to the measurement uncertainty ($\sim 3.5\%$ of the full scale). The slight peak close to the porous layer results from the outgoing flux, previously mentioned. Note that the average vertical velocity v is zero because of the impervious upper and lower walls of the cell.

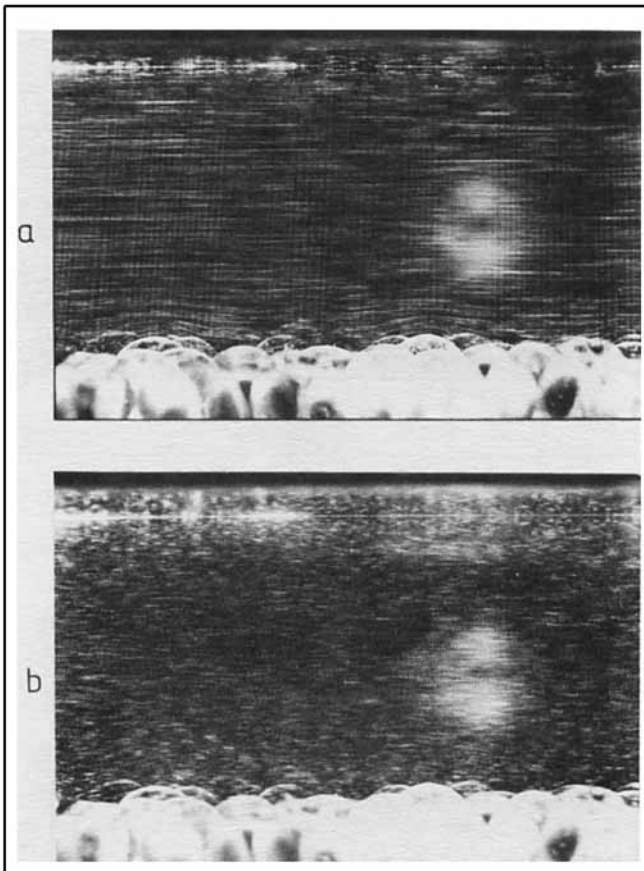

Figure 6. Flow between a solid wall and a bed of 10 mm glass beads.

Longtime exposure (a) and multiexposure with a velocity shift; (b) photographs.

Beds of spherical particles

Since the surface of these media is irregular at the grain size scale (Figure 6a), an averaging volume larger than in the previous case is needed. Therefore, several parallel vertical cross sections were investigated. With the larger beads ($\phi = 10$ mm), four pictures separated by two mm were recorded. The distance from the front side wall of the cell ranged from 50 to 56 mm. With the smaller beads ($\phi = 6$ mm), 10 planes, separated by 1.5 mm, were used. They were located between 60 and 73.5 mm from the side wall. In both cases, the longitudinal dimension of the pictures was about 70 mm. Thus, the horizontal areas of the domains of investigation were 420 mm^2 and 1,050 mm^2, respectively.

The velocity shift technique was implemented for these measurements. The photo camera was translated during the exposure with a constant upstream velocity $v_s = 1$ mm/s. Thus, the apparent velocity range in the flow was $1 \sim 4$ mm/s, and the velocities could be measured throughout the channel on a single picture at each location (Figure 6b). The beam-sweep frequency was set to $f = 10$ Hz and the exposure time to 0.5 s.

The local velocities were measured along successive horizontal lines, separated by $\delta = 1.024$ mm ($\phi = 10$ mm) or $\delta = 1.000$ mm ($\phi = 6$ mm). The number of points per lines was adapted to the flow pattern at their elevation. In the upper part of the channel, the streamlines are almost linear, and the velocity was only measured at 14 serial points, with separations equal to 5δ. In the lower part, the flow pattern is irregular and 70 points (spacing of δ) were investigated. In the intermediate region, 35 points, with a 2δ spacing, were taken into account. The relative thicknesses of these layers were different for the two beds, since they have different roughnesses.

The average longitudinal component of the velocity $\overline{u}$ is plotted in Figures 7a and 8a. As seen in Figure 6, some parts of the measurement domain are hidden by beads located above the average boundary. These missing measurements were ignored in the averaging process. In the present situation, it makes no sense to try to define an interface between the free flow and the porous medium. Instead, there is a continuous variation of the areal porosity, from 1 in the clear fluid to 0.34 or 0.40 in the bulk of the porous layer. This areal porosity is plotted in the same figures, as far as it could be measured on the photograph. The root mean square vertical component of the velocity is plotted in Figures 7b and 8b.

Again, parabolic velocity profiles were fitted, by a least-

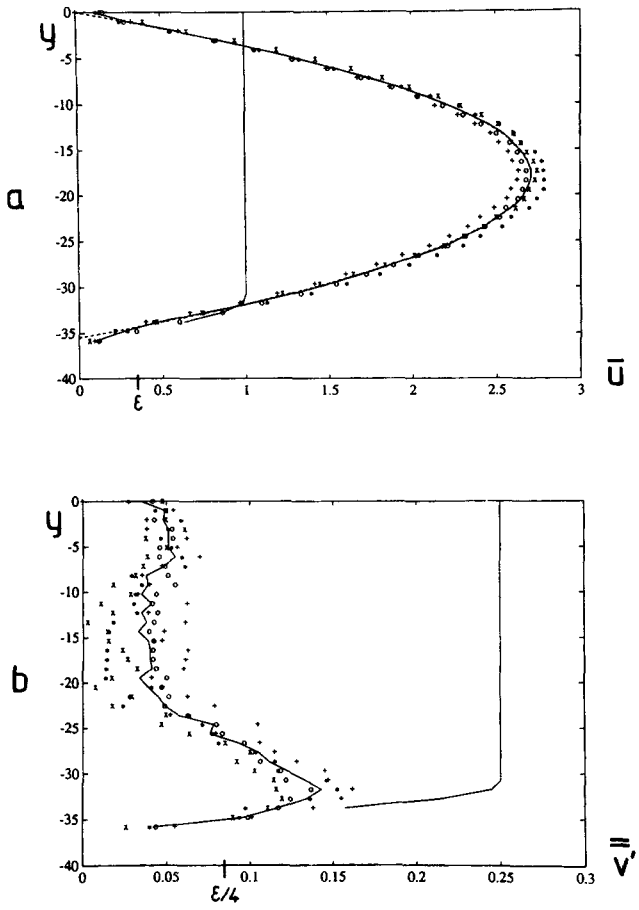

Figure 7. Flow between a solid wall and a bed of 10 mm glass beads. Distances are in mm and velocities in mm/s.

(a) Average longitudinal velocity $\bar{u}$. The symbols are averages along horizontal lines in a single plane. The solid line is the overall average. The dash line is a fitted parabolic profile. The areal porosity is also displayed. The porosity in the bulk of the bed is indicated on the x axis; (b) Standard deviation of the vertical velocity $\bar{v}'$; conventions are the same as in a. The areal porosity is divided by 4.

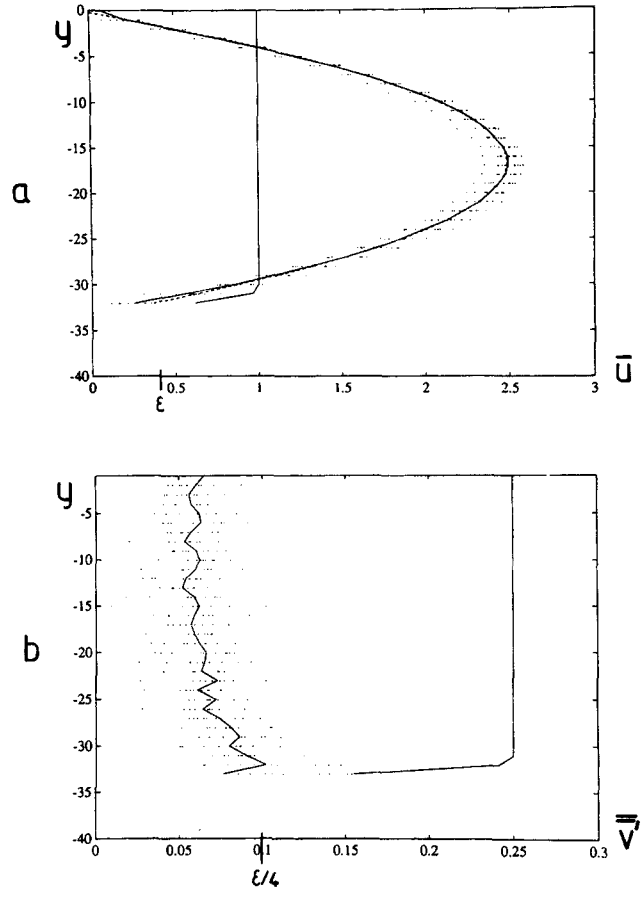

Figure 8. Flow between a solid wall and a bed of 6 mm glass beads.

Conventions are the same as in Figure 7.

square method, on the data for the upper part (25 mm) of the channel, where the streamlines are fairly rectilinear, as seen in Figures 7b and 8b. The average longitudinal velocities are indeed very precisely distributed along these profiles, which are plotted in dotted lines in Figures 7a and 8a. Slight discrepancies occur only when the areal porosity is sensibly smaller than unity. We shall not elaborate on the data in this region because they may be statistically biased because of the opacity of the medium. The data of the next subsection are more reliable in this respect.

These profiles could be successfully compared to Brinkman equation by using $\tilde{\mu}=\mu$ and $2h=32.9$ mm ($\phi=6$ mm) or $2h=35.6$ ($\phi=10$ mm) in Eq. 7a.

Since the location of an idealized interface between the channel and the porous layer cannot be defined in an intrinsic manner, it made little sense to apply Beavers and Joseph's model (Eq. 4). Note that the constant α is found to be positive only if the interface is below the highest solid point by at most one sphere radius.

The vertical velocity fluctuation profiles are very similar for the two beds (Figures 7b, 8b). There is a wide plateau in the upper part of the channel. In this region, the streamlines are almost linear and this plateau corresponds to the noise level of the measurement (~2% of the full scale in both cases). Conversely, there is a maximum close to the porous medium. The ordinate of the maximum coincides with the horizontal plane where the areal porosity starts decreasing, that is, with the top of the highest spheres. Then, the velocity fluctuations decrease regularly. They reach the noise level at about one bead diameter above the boundary. The maximum intensity of the fluctuations above the noise level seems to be roughly proportional to the gain size: 3.3% of u_M for $\phi=10$ mm and 1.6% of u_M for $\phi=6$ mm.

By way of illustration, the complete velocity field, measured in a vertical cross-section of the flow above the bed of 10 mm spheres is presented in Figure 9a. The same data, relative to the average values for each elevation (symbols on Figure 7) are presented in Figure 9b.

Beds of random particles

These random media have a very irregular structure. For this reason, measurements were performed in several parallel planes, 4 for the broken rods, and 3 for the broken plates, with a 6 mm spacing. The longitudinal dimension of the windows was about 70 mm. Hence, the horizontal areas of the

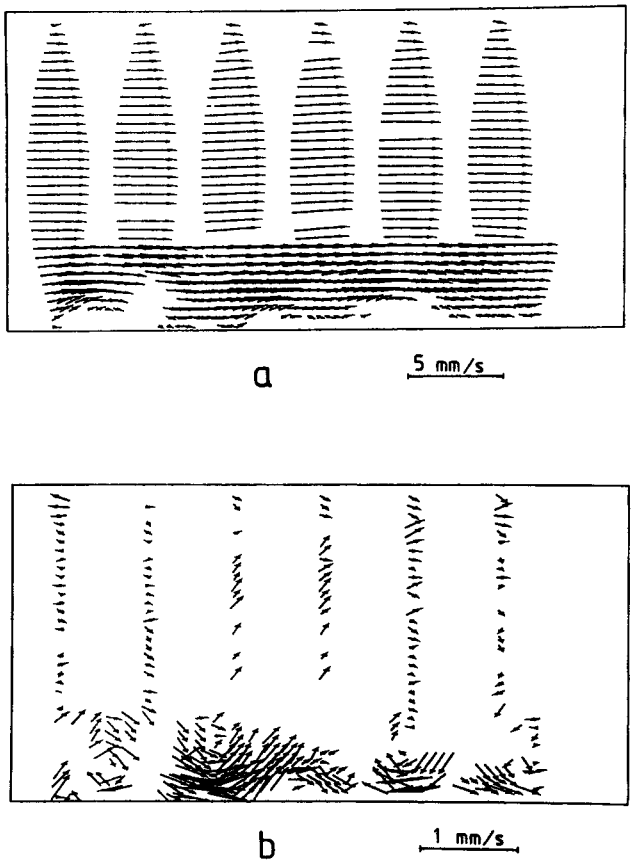

Figure 9. Flow between a solid wall and a bed of 10 mm glass beads.

Local velocity field (a), and fluctuations with respect to the average vertical profile (b).

domains of investigation were 1,680 and 1,260 mm^2, respectively, that is, about 2×7 typical grain diameters. Figures 10 and 11 display long-time exposure photographs of the investigated sections. Again, the velocity shift technique was used,

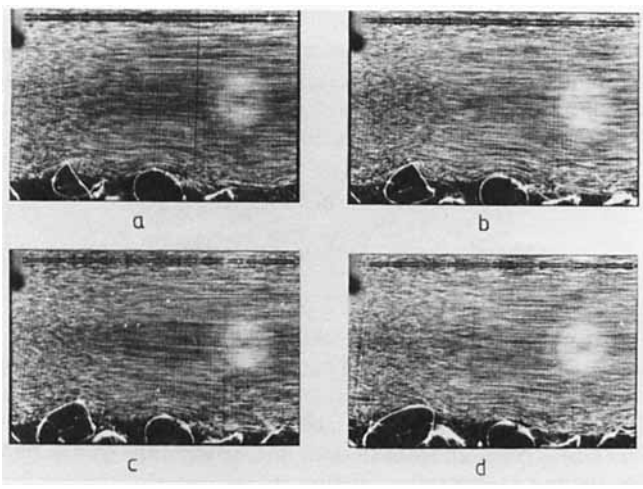

Figure 10. Flow between a solid wall and a bed of randomly broken rods.

The four cross sections (a, b, c, d) are separated by 6 mm.

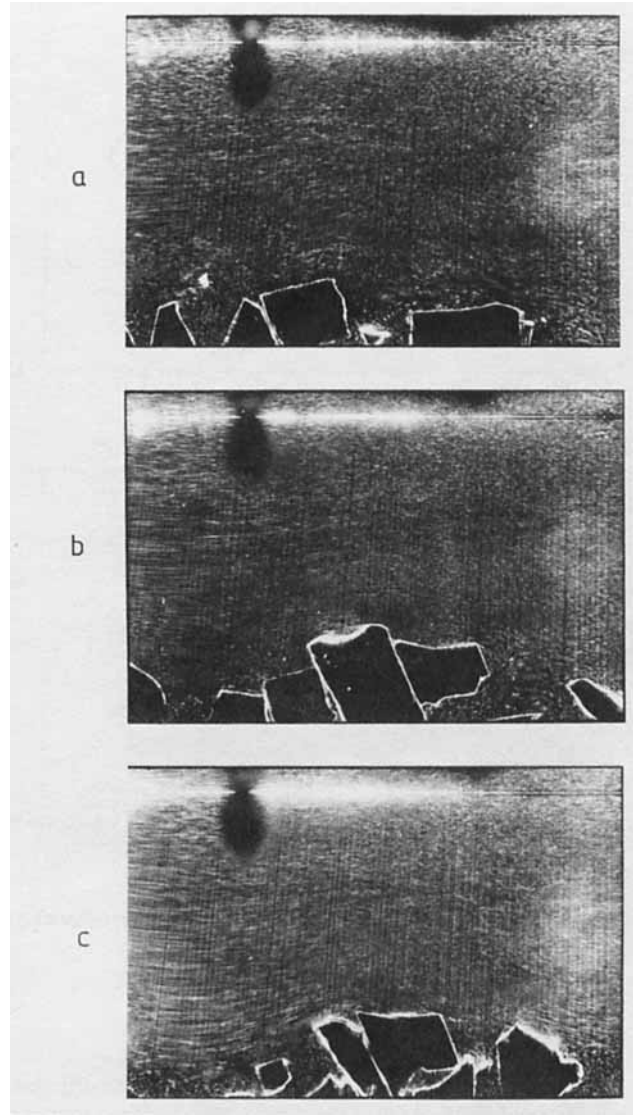

Figure 11. Flow between a solid wall and a bed of randomly broken glass plates.

The three cross sections (a, b, c) are separated by 6 mm.

with a countervelocity $u_s = 1$ mm/s. The beam-sweep frequency was $f = 10$ Hz and the exposure time 0.5 s.

In contrast with the previous materials, these media could be made transparent by matching the refractive indices of the fluid and solid phases. Consequently, the solid beads located between the measurement plane and the camera did not prevent the passage of light, and velocity could be measured between the upper grains of the porous layer. The local velocities were again measured on successive horizontal lines, separated by $\delta = 0.907$ mm (rods) or $\delta = 0.969$ mm (plates). The number of measurements per line was set to 70 and 35 in the lower and upper halves of the channel, respectively. This corresponds to separations of δ and 2δ.

The average longitudinal component $\overline{u}$ of the velocity is plotted in Figures 12a and 13a. The areal porosity, measured on the photographs of Figures 10 and 11, is also displayed. The root mean square fluctuation of the vertical velocity $\overline{v'}$ is plotted in Figures 12b and 13b.

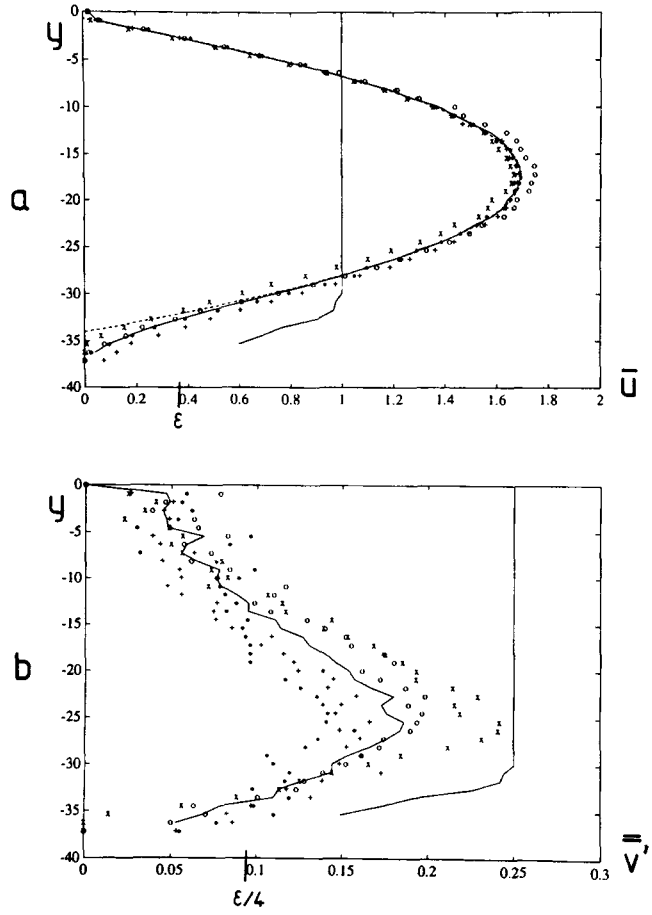

Figure 12. Flow between a solid wall and a bed of broken glass rods.

Conventions are the same as in Figure 7.

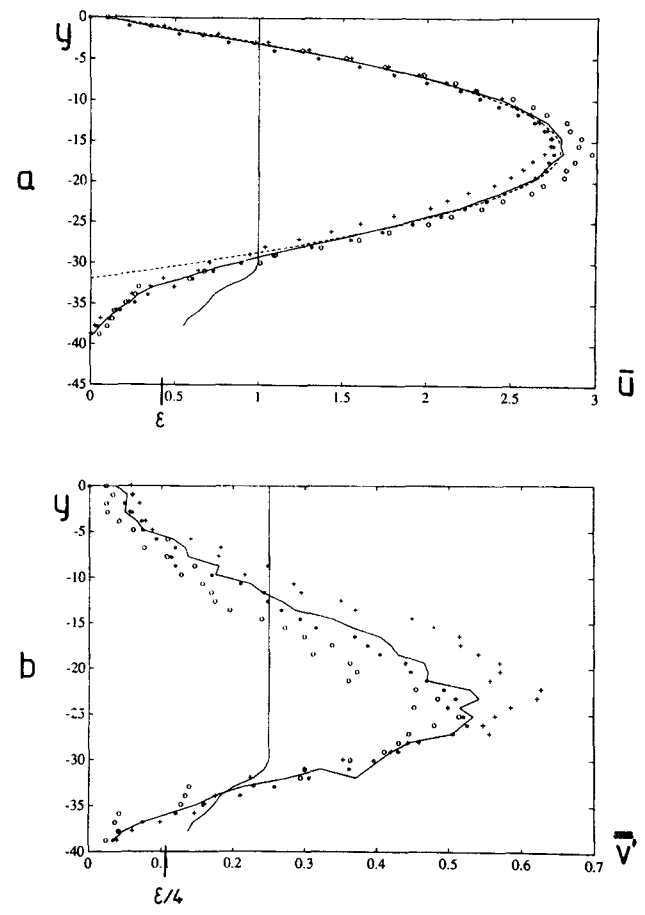

Figure 13. Flow between a solid wall and a bed of broken glass plates.

Conventions are the same as in Figure 7.

Again, a parabolic velocity profile was fitted on the data for the longitudinal velocity. Since the streamlines are nowhere straight lines (see Figures 12, 13), the fit was done in the region where the areal porosity is unity (~30 mm upper layer). It appears that even though the flow in the channel is strongly disturbed by the protruding solid grains, the average longitudinal velocity is accurately represented by a parabolic profile, for both types of media. However, below the level of the highest particle, a significant departure is observed.

As in the previous case, the Beavers and Joseph's model (Eq. 4) was not applied, because the location of the interface could not be clearly defined.

Let us examine these data in the context of the Brinkman equation. We assume here that the porous media are isotropic and homogeneous, at least in the horizontal directions, and that the averaging domain is large enough. Under these conditions:

$$v = \begin{pmatrix} u(y) \\ 0 \\ 0 \end{pmatrix} \qquad \nabla p = \begin{pmatrix} G \\ 0 \\ 0 \end{pmatrix} \tag{12}$$

where y is the vertical direction and x is parallel to the main flow. The Brinkman equation yields:

$$\frac{\tilde{\mu}}{\mu} u'' - \frac{u}{K} = u_0'' = \frac{G}{\mu} \tag{13}$$

where u'' is the second derivative of u, and u_o'' the constant value of u'' in the upper part of the channel, assuming that the upper wall is far enough to allow the existence of such a region. This is indeed the case here, as shown by the good fit by a parabolic profile. These fitted profiles yield:

$$\begin{aligned} u_o'' &= -12.2 \quad \mathrm{m^{-1} \cdot s^{-1}} \text{ (rods)} \\ u_o'' &= -21.5 \quad \mathrm{m^{-1} \cdot s^{-1}} \text{ (plates)} \end{aligned} \tag{14}$$

Before examining the data, let us describe what was expected. As already stated, u'' should be constant in the upper part of the channel. Conversely, in the bulk of the porous medium, u'' should vanish. In the intermediate region, an inflexion point ($u'' = 0$) is required for a smooth link between the Stokes parabolic and Darcy's flat profiles. Consequently, the vertical profile for u'' should be of the type displayed in Figure 14. Also, the Darcy's velocity u_D in the bulk of the porous layer is expected to be:

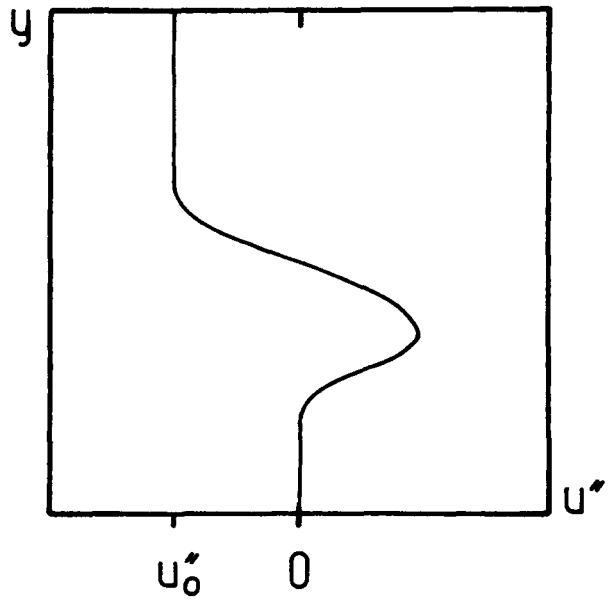

Figure 14. Typical profile of the second derivative of the longitudinal velocity $u'' = \partial^2 u / \partial y^2$.

$$u_D = -Ku_o'' \tag{15}$$

that is, with the current values of K and u_o''

$$\begin{aligned} u_D &= 1.2 \quad \mu\text{m}\cdot\text{s}^{-1} \text{ (rods)} \\ u_D &= 2.2 \quad \mu\text{m}\cdot\text{s}^{-1} \text{ (plates)} \end{aligned} \tag{16}$$

The lowest velocities reported in Figures 12 and 13 are 0.041 mm/s and 0.022 mm/s, respectively; this suggests that the domain of investigation did not contain the region of established Darcy flow with a constant seepage velocity. The same conclusion can be drawn from the plot of u'' in Figures 15a and 16a. It is well known that the differentiation of experimental data always introduces a significant noise level, especially for second-order derivatives like u'' which was deduced locally from the values of u at successive measurement points. A slight smoothing was then performed by a convolution technique. Although the data are somewhat scattered, a pattern similar to Figure 14 is clearly observed. The plateau in the channel and the inflexion point are visible. In both cases however, the lower region with vanishing u'' lies beyond the domain of investigation; it means that the intermediary layer extends deeper than one typical grain size beneath the top of the solid grains. Note that this depth is much larger than $\sqrt{K} \sim 0.3$ mm. For the broken rods the inflection point of u is at the level of the highest solid, whereas it is slightly higher (~ 3 mm) for the broken plates. This may result from the presence, in the latter case, of solid particles out of the averaging domain which are still higher than those inside it. Their shadows are hardly visible in Figure 11. They are not taken into account in the measured areal porosity, but they nonetheless influence the flow in the measurement domain. This simply means that the horizontal extent of the domain of investigation is not large enough.

Suppose now that we attempt to describe the experimental

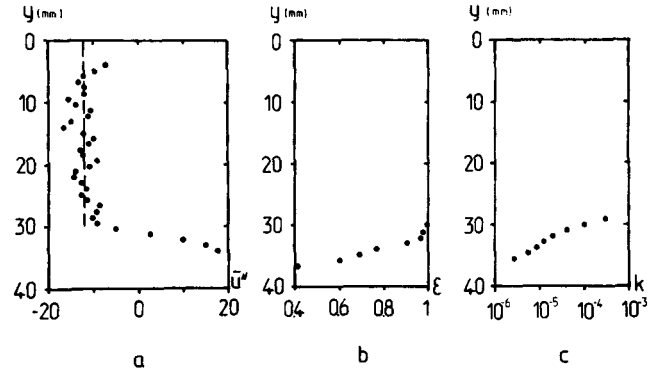

Figure 15. Flow between a solid wall and a bed of broken rods.

(a) Second vertical derivative of the longitudinal velocity in $m^{-1}\cdot s^{-1}$; the dash line is deduced from the fitted profile in Figure 12a; (b) areal porosity; (c) permeability, as deduced from Eq. 18 in m^2.

data by Eq. 13, with a stepwise function for K. This requires in turn a stepwise profile for $\tilde{\mu}/\mu$. Above an (arbitrary) level, $\tilde{\mu}/\mu = 1$. Beneath it, $\tilde{\mu}/\mu$ rised to much larger and fluctuating values, in the 100 ~ 1,000 range. This is obviously not satisfactory.

Alternatively, let us assume $\tilde{\mu} = \mu$ and a discontinuous permeability. The profiles (Eq. 7a) can be fitted to the experimental data with $2h = 33.1$ mm (rods) or $2h = 31.5$ mm (plates). Consequently, Eq. 7b provides the following velocity profiles in the porous layers:

$$u = 1.22\ 10^{-6}[1 + 10^7 e^{(y - 33.1\ 10^{-3})}] \quad \text{(rods)} \tag{17a}$$

$$u = 2.15\ 10^{-6}[1 + 10^7 e^{(y - 31.5\ 10^{-3})}] \quad \text{(plates)} \tag{17b}$$

These profiles are not in good agreement with the data both in the free fluid and in the porous medium sides. In particular, the range of the parabolic profile and the subsequent exponential decay are overpredicted by Eq. 7.

Therefore, it seems necessary to take into account a variation of the permeability in an intermediate layer. Moreover, $\tilde{\mu}$ is not expected to be very different of μ. If, for example, the effective viscosity is taken as μ/ϵ, $\tilde{\mu}/\mu$ is still of the order of

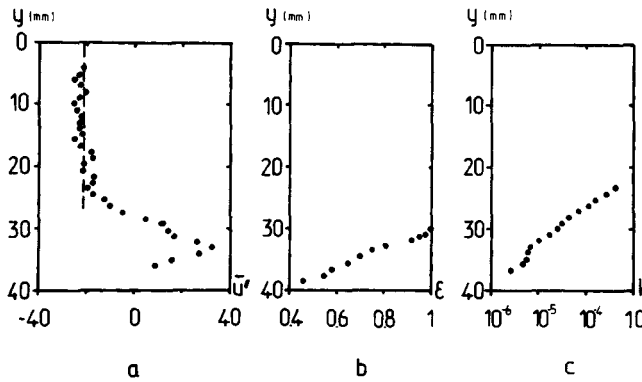

Figure 16. Flow between a solid wall and a bed of broken plates.

Conventions are the same as in Figure 15.

unity. Suppose then $\tilde{\mu}/\mu = 1$. Then the permeability, according to Eq. 13, is given by:

$$K = u/(u'' - u_o'') \tag{18}$$

This result is plotted in Figures 15c and 16c for both materials. A smooth variation of K is observed in both cases. Again, the bulk value of K is not reached in the measurement domain. The computed permeability grows regularly as one goes up to the upper wall and diverges as one leaves the porous layer, as expected on physical grounds.

The averaging domain in these experiments is too limited, both in its depth and in its horizontal extent, to be much more specific. However, the present data show clearly that when the Brinkman's equation is used around the boundary of a random porous medium, the precise definition of the effective viscosity is secondary and the variations of permeability are predominant.

Finally, consider the vertical velocity fluctuations. Several comments can readily be made in Figures 12 and 13. First, the fluctuation intensity is much larger than for the previous media, since it can reach $\sim 10\%$ (rods) or $\sim 20\%$ (plates) of u_M. This illustrates the obvious fact that $\overline{v'}$ is an increasing function of the roughness of the surface. Second, the maximum is located slightly above the level of the highest solid in the domain. Again, this may result from the presence of still higher particles on both sides of the measurement volume. Third, no plateau is obtained in the upper part of the channel. In these two cases, the channel is too shallow and the disturbance induced by the porous layer interacts with the upperwall. It is expected that in a deeper channel the decay of $\overline{v'}$ toward the solid wall would be slower. Note that the width of the maximum is several times larger than the grain size.

Concluding Remarks

In view of our data, and as often pointed out in the literature, both the Beavers and Joseph model (Eq. 4) and the Brinkman Eq. 6 face the same problem, namely the determination of the location where Eq. 4 or the step of K in Eq. 6 is to be applied. The location of this equivalent interface is *a priori* unknown and can only be set, when the surface boundary is examined, with an uncertainty of the order of the roughness, that is, of the grain size. On the other hand, since both models yield a correction for the longitudinal velocity component in the channel which corresponds to a shift of the boundary of order $\sqrt{K}$, which is generally much smaller than the grain size, one may question whether their application yield more accurate results than a simple no-slip condition at some reasonable but otherwise arbitrary location.

As far as the longitudinal flow in the superficial layer of the porous medium is concerned neither model provide satisfactory predictions. Of course, the Beavers and Joseph condition, which is essentially macroscopic, yields a flat velocity profile up to the idealized interface. The correction term to Darcy's Law in the Brinkman equation indeed induces an exponential decay, but unless the surface of the medium has been machined so that permeability is discontinuous, this decay is much too steep, as shown above. Our data suggest that a more realistic description could be achieved by using a position dependent permeability in the Brinkman equation, provided that a detailed knowledge of the geometry of the medium near its boundary is available, and provided that it could be related to the varying permeability.

Considerations about the transverse component of the velocity, which is totally ignored in both Beavers and Joseph and Brinkman's models, might be much more fruitful. Due to the roughness of the boundary, spatial fluctuations of the normal velocity are observed, even though they average to zero. The disturbance extends up to a few grain sizes in the outer flow.

If the free flow and the porous medium are not in thermal or solutal equilibrium, the vertical velocity fluctuations will induce convective heat or solute exchanges between the two domains, which could possibly exceed the diffusive exchanges. At a mesoscopic scale (that is, the scale where the Brinkman equation with a position dependent permeability is written), this transfer enhancement can probably be described by an effective diffusivity, similar to the one introduced in turbulent flows. At a macroscopic scale, this might result in a net flux proportional to the concentration step and to the flow intensity, with a prefactor which depends on the geometry of the porous medium. This would yield a boundary condition for the concentration similar to the Beavers and Joseph model for the momentum. This point will be further investigated in future works.

Literature Cited

Adler, P. M., "Hydrodynamic Properties of Fractals Flocs," *Faraday Disc. Chem. Soc.*, **83**, 145 (1987).

Beavers, G. S., and D. D. Joseph, "Boundary Conditions at a Naturally Permeable Wall," *J. Fluid Mech.*, **30**, 197 (1967).

Berker, R., *Encyclopedia of Physics: Fluid Dynamics II*, S. Flugge and C. Truesdell, eds., **8.2**, Springer-Verlag, Berlin (1963).

Brinkman, R., "A Calculation of the Viscous Force Exerted by a Flowing Fluid on a Dense Swarm of Particles," *Appl. Sci. Res.*, **A1**, 27 (1947).

Landreth, C. C., and R. J. Adria, "Electrooptical Image Shifting for Particle Image Velocimetry," *Appl. Opt.*, **27**, 4216 (1988).

Larson, R. E., and J. J. L. Higdon, "Microscopic Flow Near the Surface of Two-Dimensional Porous Media. I—Axial Flow," *J. Fluid Mech.*, **166**, 449 (1986).

Larson R. E., and J. J. L. Higdon, "Microscopic Flow Near the Surface of Two-Dimensional Porous Media. II—Transverse Flow," *J. Fluid Mech.*, **178**, 119 (1987).

Lundgren, T. S., "Slow Flow through Stationary Random Beds and Suspensions of Spheres," *J. Fluid Mech.*, **51**, 273 (1972).

Masliyah, J. H., and M. Polika, "Terminal Velocity of Porous Spheres," *Can. J. Chem. Eng.*, **58**, 299 (1980).

Matsumoto, K., and A. Suganuma, "Settling Velocity of a Permeable Model Flow," *Chem. Eng. Sci.*, **32**, 445 (1977).

Prat, M., "Modélisation des Transferts en Milieux Poreux. Changement d'échelle et Conditions aux Limites," PhD Thesis, Toulouse (1989).

Richardson, S., "A Model for the Boundary Condition of a Porous Material," *J. Fluid Mech.*, Part 2, **49**, 327 (1971).

Rumpf, H., and A. R. Gupte, "Einflüsse der Porosität und Korngrössen Verteilung in Widerstandsgesetz der Porenströmung," *Chem. Ing. Tech.*, **43**, 367 (1971).

Saleh, S., J. F. Thovert, and P. M. Adler, "Measurement of Two-Dimensional Velocity Fields in Porous Media by Particle Image Displacement Velocimetry," *Exp. in Fluids*, **12**, 210 (1992).

Saleh, S., "Etude Expérimentale d'écoulements à l'intérieur et Autour de Milieux Poreux par Vélocimétrie par Images de Particules," PhD Thesis, Paris (1993).

Taylor, G. I., "A Model for the Boundary Condition of a Porous Material," *J. Fluid Mech.*, Part 1, **49**, 319 (1971).

Vignes-Adler, M., P. M. Adler, and P. Gougat, "Transport Processes along Fractals. The Cantor-Taylor Brush," *Phys. Chem. Hydro.*, **8**, 401 (1987).

Manuscript received Oct. 20, 1992, and revision received Apr. 5, 1993.